
Evaluation of ^{11}C -Colchicine for PET Imaging of Multiple Drug Resistance

Andre Levchenko, Bipin M. Mehta, Jong-Bin Lee, John L. Humm, Finn Augensen, Olivia Squire, Paresh J. Kothari, Ron D. Finn, Edward F. Leonard, and Steven M. Larson

Nuclear Medicine Research Laboratory and Service, Department of Medical Physics, and Radiochemistry Laboratory, Memorial Sloan-Kettering Cancer Center, New York; and Center for Biomedical Engineering, Columbia University, New York, New York

Overexpression of P-glycoprotein (P-gp) can confer multiple drug resistance (MDR) phenotype on cancer cells and tumors by reducing intracellular accumulation of various cytotoxic agents. Early diagnosis of MDR in the clinic will serve to improve the efficacy of chemotherapeutic intervention and the quality of life of patients. In this article we describe use of a positron-emitting MDR tracer, ^{11}C -colchicine (CHC), to evaluate MDR by PET imaging. Unlike existing MDR tracers such as $^{99\text{m}}\text{Tc}$ -sestamibi, this compound is electroneutral, with biodistribution not affected by perturbations of membrane potential. **Methods:** In vitro studies showed that resistance to CHC is correlated to resistance to Taxol (paclitaxel). The results of biodistribution experiments were found to be consistent with previously reported experiments with CHC labeled with other isotopes. On the basis of in vitro experiments with a series of drug-resistant variants of the human neuroblastoma BE (2)-C cell line, a mathematic model of ^{11}C -CHC distribution in tumors was formulated. Dynamic PET ^{11}C -CHC imaging experiments were performed with nude rats xenografted with the BE (2)-C-sensitive and -resistant strains. Each scan was accompanied by a transmission scan and a static FDG scan. These scans allowed improved image localization. **Results:** We observed an approximately 2-fold difference between ^{11}C -CHC accumulation in sensitive and resistant tumors. Imaging data were analyzed using the mathematic model, and various parameters characterizing resistance could be identified and estimated. In particular, the parameter r , proportional to the level of resistance of the tumors, was obtained. We showed that the ratio of these r parameters determined from the sensitive and resistant tumors was identical to the ratio of CHC accumulation in the corresponding sensitive and resistant cell lines used for xenografting. **Conclusion:** These in vivo experiments provided additional evidence for the indirect effect of P-gp action on CHC-to-tubulin binding, which in turn determines CHC uptake in tumors. The significance of these findings and future plans is discussed.

Key Words: multiple drug resistance; colchicine; PET; mathematic model

J Nucl Med 2000; 41:493–501

Multiple drug resistance (MDR) describes the propensity of cancer cells to resist the actions of various chemically and functionally unrelated substances including, but not limited to, chemotherapeutic agents. Several biochemical mechanisms have been shown to confer the MDR phenotype, the most studied of which mechanisms is overexpression of P-glycoprotein (P-gp) (1–7). In cases of breast and kidney cancer, hematologic malignancies, childhood neuroblastoma, and osteosarcoma, a correlation between P-gp expression and poor treatment prognosis has been shown (8–16).

P-gp is the 170-kDa, 1280-amino acid product of the *mdr1* gene, found on the long arm of chromosome 7 (17). According to its amino acid sequence, P-gp is classified as a member of the adenosine triphosphate (ATP)-binding cassette superfamily of transmembrane transporters. This family includes among its many members cystic fibrosis transmembrane regulator, MDR-associated protein, and class I antigen presentation transporter. Topologically, P-gp consists of 2 homologous sets of 6 hydrophobic transmembrane domains, each followed by a single ATP-binding site, and thus forms a functional heterodimer (18,19). Overexpression of P-gp may result in increased excretion and decreased retention of various MDR substrates and decreased cytotoxic efficacy of anticancer agents.

Until recently, clinical evaluation of MDR and P-gp expression has been confined to analysis of tumor biopsies using a variety of techniques, such as immunohistochemistry, quantitative autoradiography, and reverse transcriptase polymerase chain reaction (4,20–22). These methods, though generally accurate, are invasive and, thus, often difficult or impossible to perform. In addition, the relevance of results obtained *ex vivo* to the physiologic situation cannot always be substantiated. These considerations have led several groups of investigators to attempt to develop noninvasive modalities for clinical diagnostic imaging of MDR.

Several radiolabeled MDR tracers have been described (7,17). In all cases investigators have used P-gp substrates as tracer candidates. A group of $^{99\text{m}}\text{Tc}$ -labeled organic cations including sestamibi, tetrofosmin, and several so-called Q-complexes (the most promising of which are Q57, Q58, and

Received Oct. 25, 1998; revision accepted Jun. 21, 1999.
For correspondence or reprints contact: Bipin M. Mehta, PhD, Nuclear Medicine Research Laboratory, Memorial Sloan-Kettering Cancer Center, New York, NY 10021.

Q63) has been shown to be excellent P-gp substrates both in vitro and in vivo (6,23–26). Resistance to sestamibi has been shown to be almost exclusively associated with membrane potential perturbations as a result of P-gp action (6). This fact makes sestamibilike compounds very attractive in modeling resistance to a variety of weakly basic or cationic P-gp substrates.

Another group of substances being tested is ¹¹C-labeled daunorubicin and verapamil, both already widely used in the clinic (27,28). An attractive feature of these tracers is their direct relevance to clinically used regimens. Because most anthracyclines are weak bases, their biodistribution is likely to be affected by both membrane potential and their affinity to the target (DNA) in resistant cells. Both these quantities may be altered by P-gp (29,30).

In this article we present the results of experiments devised to test ¹¹C-labeled colchicine ([CHC] Fig. 1) as a marker of resistance to electroneutral P-gp substrates. We have been encouraged to use ¹¹C-CHC by the results of previously reported biodistribution studies that confirmed that CHC uptake is significantly lower in resistant versus sensitive tumors (31–33). CHC is attractive as a potential MDR tracer, because it has a clearly identified intracellular target (tubulin subunits) and because it is relatively easy to label at a carbon atom.

In a separate report we presented a theoretical treatment of the mechanism of P-gp-mediated resistance to CHC (unpublished data). The mathematic analysis was verified by in vitro experiments in which the relationship between CHC uptake, P-gp expression, and level of resistance was studied. Here, we modify this analysis to model in vivo CHC uptake in xenografts obtained from the tumor cells studied in vitro. A major assumption underlying this study is that P-gp expression remains invariant when cells are grown in vivo.

MATERIALS AND METHODS

Mathematic Analysis

The notation used in the analysis of colchicine uptake in sensitive and resistant tumors in vivo is summarized in Table 1. The

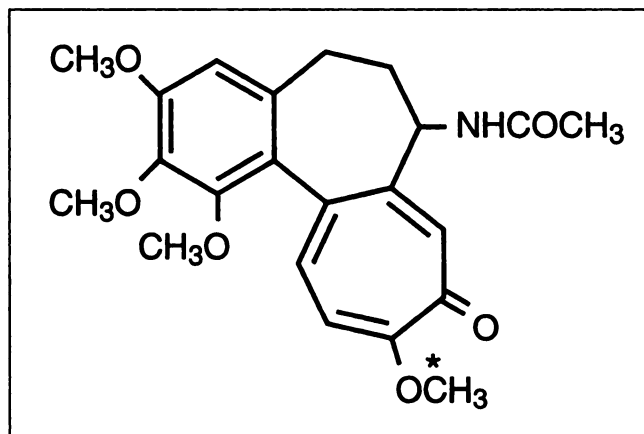


FIGURE 1. Structure of CHC is shown with asterisk denoting ring C methoxy carbon. This position of ¹¹C label was used in all experiments.

TABLE 1
Terms Used in Mathematic Analysis

Term	Definition
c_i	Concentration of free colchicine inside cell
c_b	Concentration of colchicine–tubulin complexes
c_o	Concentration of colchicine outside cell
T	Concentration of free tubulin subunits
P	Number of P-gp molecules in cell membrane
t	Time
k_1	Constant of forward colchicine–tubulin reaction
k_2	Constant of reverse colchicine–tubulin reaction
k_b	Rate of colchicine plasma clearance

following equation takes into account passive CHC diffusion (CHC is not charged) and binding of CHC to tubulin. In a separate study, the contribution of P-gp to resistance was found to be primarily indirect, resulting in altered affinity to the intracellular target rather than direct transport. Thus:

$$\frac{dc_i}{dt} = k(c_o - c_i) - k_1c_iT + k_2c_b. \quad \text{Eq. 1}$$

The equation describing the kinetics of bound CHC is:

$$\frac{dc_b}{dt} = k_1c_iT - k_2c_b. \quad \text{Eq. 2}$$

We will assume that the transport of CHC through the cell membrane is much faster than its rate of binding to tubulin. Binding to tubulin is thus rate limiting, so:

$$k(c_o - c_i) \cong 0, \quad \text{Eq. 3}$$

or

$$c_i = c_o, \quad \text{Eq. 4}$$

at the time scale determined by CHC–tubulin binding. Assuming that the extracellular CHC concentration is determined by CHC blood clearance and can be approximated by an exponential decay:

$$c_o = C_o \exp(-k_b t), \quad \text{Eq. 5}$$

where k_b is the rate of CHC clearance from plasma. Substituting Equations 4 and 5 into Equation 2, we have:

$$\frac{dc_b}{dt} = k_1T C_o \exp(-k_b t) - k_2c_b. \quad \text{Eq. 6}$$

The general solution of the homogeneous part of this differential equation is:

$$c_b = C \exp(-k_2 t). \quad \text{Eq. 7}$$

Substituting this solution into Equation 6 and assuming that the constant C is time dependent, then:

$$C = \frac{k_1T C_o}{k_2 - k_b} \exp((k_2 - k_b)t) + C_1, \quad \text{Eq. 8}$$

$$c_b = \frac{k_1T C_o}{k_2 - k_b} \exp(-k_b t) + C_1 \exp(-k_2 t). \quad \text{Eq. 9}$$

Because at time $t = 0$ the bound CHC concentration $c_b = 0$, Equation 9 yields for this initial condition: where C_1 is a constant to be determined from the initial conditions ($t = 0$). Substituting Equation 8 into Equation 7:

$$c_b = \frac{k_1 T C_0}{k_2 - k_b} [\exp(-k_b t) - \exp(-k_2 t)]. \quad \text{Eq. 10}$$

It is evident that if the CHC plasma concentration becomes significantly lower than the concentration of CHC-tubulin complexes, the bound concentration is described by dissociation of CHC from tubulin:

$$c_b = -k_2 c_b, \quad \text{Eq. 11}$$

or

$$c_b = c_b(0) \exp(-k_2 t). \quad \text{Eq. 12}$$

Equations 10 and 12 were used in the analysis of experimental data.

Cell Lines

The cell lines used in this study were the human neuroblastoma cell line BE (2)-C and its resistant strains: CHC-10', CHC-100', CHC (0.2 $\mu\text{g}/\text{mL}$), and CHC (1 $\mu\text{g}/\text{mL}$). These strains were developed by selection for resistance to 25, 250, 500, and 2500 nmol, respectively, of CHC. Cells were maintained as monolayers in high glucose Dulbecco's modified medium with essential amino acids (DME) supplemented with 10% fetal calf serum and 2% penicillin/streptomycin, in a humidified atmosphere with 5% CO_2 . Cells were passaged 1 to 2 times each week to maintain exponential growth. The resistant cell line was periodically challenged with CHC at concentrations used for selection to ascertain the constant level of resistance. The resistance levels were found to be constant for at least 3 mo with no CHC present in the growth culture.

Determination of Level of Resistance

For determination of the level of resistance, cells were grown for 3 d in 24-well plates in the presence of varying concentrations of CHC and Taxol (paclitaxel). The number of cells in each well was determined and expressed as a percentage of the number of cells in the wells in which no drug was present. These data were plotted as a function of the corresponding drug concentrations. The drug concentration at which cell growth was equivalent to 50% of control (IC_{50}) was determined.

Quantitative Flow Cytometry

The monoclonal antibody MRK-16 (provided by T. Tsuruo of the University of Tokyo, Japan) directed against P-gp was used in binding studies. The antibody was purified by protein A affinity chromatography from FCS-free cultured medium as described previously by T. Tsuruo (oral communication, 1998). Cellular microbeads were obtained as part of a microbeads kit (QSC-100; Sigma Biosciences, St. Louis, MO). They consisted of 4 microparticle subpopulations of 8.2- μm diameter possessing 8,692, 20,689, 73,557, and 205,488 binding sites per bead. The binding sites were composed of covalently bound goat antimouse antibodies reactive against mouse IgG2a isotype. For quantitative flow cytometry assays, a slight modification of the method of Ferrand et al. (34) was used. Briefly, cells were harvested in the mid to late exponential growth phase by scraping and resuspending at a final concentration of 10^7 cells/mL in the reaction medium (DME supplemented with 2% rabbit serum). Aliquots of 100 mL were then taken from

the cell suspension and placed into 1 mL Eppendorf tubes. The microbeads were simultaneously resuspended in the reaction medium at the same concentration, and 100 mL were aliquoted into Eppendorf tubes. Then the murine anti-P-gp monoclonal antibody MRK-16 and the irrelevant antibody of the same isotype (mouse IgG2a, used as a negative control) were added to the tubes at a concentration of 20 mg/120 mL. The cells were then incubated for 45 min at 4°C. After incubation the cells were washed twice with ice-cold phosphate-buffered saline (PBS) and resuspended in 50 mL fluorescein-conjugated AffiniPure Goat AntiMouse IgG (H+L) (Jackson ImmunoResearch Laboratories, West Grove, PA) at a final antibody concentration of 7.5 mg/50 mL. The cells were then incubated in the dark for 45 min at 4°C. Cells then were washed twice with ice-cold PBS, resuspended in 300–500 mL PBS and analyzed in an EPICS Profile II cell cytometer (Beckman-Coulter, Fullerton, CA).

Animals

Immunosuppressed BALB/c mice (20–25 g body weight) and mu/mu nude rats (approximately 200 g body weight) (Harlan Sprague Dawley Inc., IN) were used in biodistribution and imaging experiments. The animals were xenografted with subcutaneous injections of 10^7 cells to initiate tumor growth. Previously, we have determined that the level of P-gp expression in tumors remains proportional to the cell lines used for xenografting (35). When tumors reached 15–20 mm (approximately 2 wk after injection), the animals were anesthetized with isoflurane (inhalation mixture of 1.25% isoflurane in pure oxygen) and prepared for experiments. After the experiments the animals were killed by lethal intravenous injection of KCl.

Radiosynthesis of ^{11}C -CHC

^{11}C -CHC was synthesized using ^{11}C -iodomethane to radiolabel desmethyl CHC, as previously described (36). The C-10 methoxy group of n-CHC was radiolabeled by this reaction. The total synthesis time was approximately 60 min, with an average specific activity of 8.88 GBq/ μmol (240 mCi/mmol). The yield of ^{11}C -CHC was 21% when corrected for end of bombardment, as described (36). As suggested by our earlier pharmacokinetics studies, the recirculated labeled metabolites of labeled CHC may be negligible (29,30).

Biodistribution Experiments

Mice were injected retroorbitally with about 3.7 GBq (100 mCi) ^{11}C -CHC. The animals were killed after 1 h, and samples of tumors, blood, brain, liver, kidney, spleen, intestines, and skeletal muscle were obtained. The samples were weighed and counted in a γ radiation counter. The procedure in rats was essentially the same. Intravenous injection was used in place of intraorbital injection. Radioactivity in counts per minute was measured by a γ counter (LKB Instruments, Gaithersburg, MD). Data were expressed in percentage injected dose (%ID) per gram of tissue.

Blood Sampling

The experimental setup for continuous and discrete blood sampling will be described elsewhere (J. Lee, unpublished data, November 1999). Briefly, the right jugular vein (JV) and left femoral artery (FA) were catheterized. Blood was passed from the FA to the JV through plastic tubing filled initially with heparin. The tubing was placed in a water jacket maintained at 37°C. Pressure detectors were attached to the tubing in proximity to the JV and the FA. A laser Doppler flow meter in proximity to the JV measured

blood flow through the tubing. The midsection of tubing passed through a coincidence detector, so that the amount of a positron-emitting isotope could be measured. This system provided measurement of real-time, ^{11}C -associated radioactivity in the blood. Data were verified by discrete blood sampling at 5, 10, 20, and 30 s and at 1, 2, 3, 5, 10, 15, 20, 30, 40, 50, and 60 min. Blood samples were weighed and counted in a γ radiation counter (LKB). All data were expressed as %ID/g.

PET

PET imaging was performed on a clinical whole-body Advance PET scanner (General Electric Medical Systems, Milwaukee, WI). The transaxial field of view was 55 cm with 14.75 cm along the axial direction. The scanner contained retractable septa and could be used in 2-dimensional mode (septa in) for high resolution imaging or in 3-dimensional mode (septa out) for higher sensitivity (1200 Hz/kBq/mL). The image resolution was 4.2 mm full width at half maximum. The Advance scanner uses a pair of ^{67}Ge rods to produce state-of-the-art attenuation correction and has dedicated software for scatter and random correction.

For PET experiments, dual (sensitive and resistant tumors in the same animal) and single tumors were grown in the neck and shoulder regions of rats. The animals were anesthetized as described above. The femoral vein was catheterized. One to 3 animals were positioned in the field of view of the camera in the same horizontal plane and were not moved throughout the experiment. At the beginning of each experiment a 10-min transmission scan was obtained. Then, 11.1–29.6 GBq (300–800 mCi) ^{11}C -CHC were injected intravenously and a 45-min dynamic emission scan was obtained. The time frames were 1 min for the first 30 min and 5 min for the rest of the study. After the dynamic emission scan 11.1–18.5 GBq (300–500 mCi) FDG were injected, and after 40 min a 10-min static emission scan was obtained.

Quantitative images were reconstructed with attenuation and scatter correction. Regions of interests (ROIs) corresponding to the tumors were identified in the FDG scans. Care was taken to identify regions with homogeneous activity throughout each ROI. The average value of FDG activity in the ROI was determined. These ROIs were then copied onto the transmission and ^{11}C -CHC scans. The geometry and size of the ROIs were preserved in the copying procedure. The transmission scan was used to verify tumor location. The average ^{11}C -CHC activity (expressed as %ID/mL) in

the ROIs was then determined for each frame and plotted as a function of time.

RESULTS

Analysis of Cell Lines

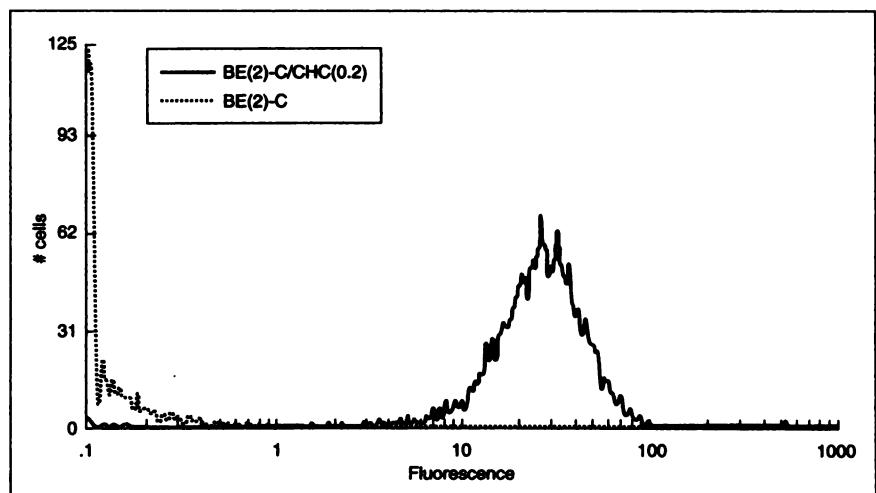
Before injection into the animals, tumor cells were analyzed by quantitative flow cytometry. A representative histogram of sensitive BE (2)-C and resistant CHC (0.2) cell lines is shown in Figure 2. P-gp concentration in sensitive cells was indistinguishable from zero. In resistant cells P-gp concentration was determined to be approximately 1.2×10^6 molecules/cell. This was in excellent agreement with the results obtained previously by the self-competitive binding assay (32). As determined by this method, P-gp expression was stable for at least 2 mo, with no drug present in the growth medium.

To determine the applicability of CHC as a tracer of another electroneutral MDR substrate, Taxol, we determined the resistance of 4 cell lines selected with different CHC-to-Taxol concentrations. We then compared IC_{50} values for growth inhibition by Taxol and CHC. The results are presented in Figure 3, showing a strong positive correlation ($R^2 = 99\%$) between resistance to CHC and resistance to Taxol.

Biodistribution Experiments

Biodistribution experiments were designed to estimate the difference between CHC uptake in sensitive BE (2)-C and resistant CHC (0.2) tumors as well as in normal tissues at a specific time point. Table 2 shows the biodistribution of ^{11}C -CHC compared with ^3H -CHC and ^{14}C -CHC (31). In the case of ^{11}C -CHC, sensitive tumors had more than twice (1.50 ± 0.16 %ID/g) the uptake of radiolabel as did resistant tumors (0.48 ± 0.09 %ID/g; $P < 0.03$). The tumor-to-blood ratio in sensitive tumors (3.59 ± 0.63) was greater than that in resistant tumors (1.07 ± 0.19 ; $P < 0.01$). Table 2 shows that for both ^3H -CHC and ^{14}C -CHC the absolute tumor and organ uptake, as well as the tumor-to-blood ratios, were

FIGURE 2. Representative overlaid flow cytometry histogram. Flow cytometry experiments were performed with anti-P-gp MRK-16 monoclonal antibody. Histogram obtained for sensitive line was indistinguishable from control histograms obtained with irrelevant isotype-matched antibody.



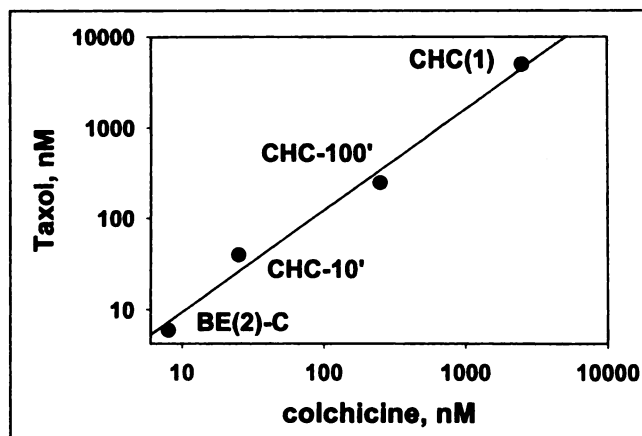


FIGURE 3. Correlation of resistance to CHC and Taxol. Results for 1 sensitive and 3 resistant cell lines are shown. Cells were allowed to grow for 3 d in presence of various drug concentrations. IC₅₀ values corresponding to drug concentrations inhibiting growth to 50% of zero concentration control were determined and plotted.

similar to ¹¹C-CHC values in sensitive as well as in resistant tumor-bearing mice. Because the PET experiments were to be performed in rats, we compared ¹¹C-CHC biodistribution in rats and mice. As is evident from Table 1, these data were found to be in good agreement.

Distribution of CHC in various organs was measured to determine the level of tissue background that can be present in PET experiments and, thus, optimal tumor placement. It was found that ¹¹C-CHC uptake in liver, kidney, and spleen was considerably higher than in both sensitive and resistant tumors. These results led to the choice of the neck and shoulder areas as locations for tumor growth.

Blood Sampling

Blood sampling experiments were performed using a continuous automated sampling technique developed in our

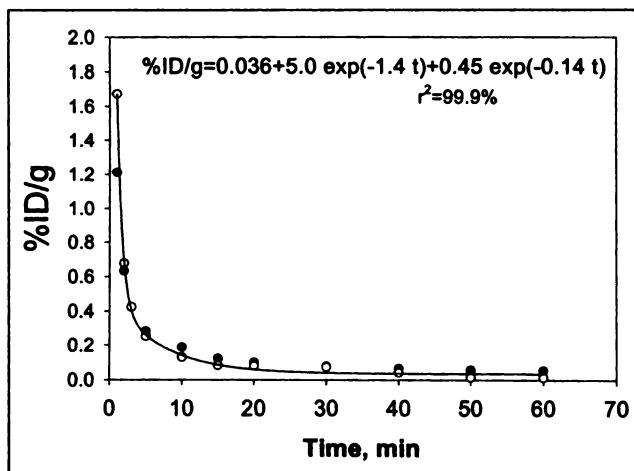


FIGURE 4. ¹¹C-CHC blood clearance. Blood was sampled continuously (○) by automatic sampling and, at several time points, manually (●) after ¹¹C-CHC bolus injection. Data were fitted with biexponential function. Correlation between continuous and manual sampling was 99%.

laboratory (unpublished data) and by discrete manual sampling (Fig. 4). The data were found to be best fitted with the biexponential curve represented by:

$$\%ID/g = 0.036(\pm 0.011) + 5.0(\pm 0.5) \exp(-1.38[\pm 0.14] t) + 0.45(\pm 0.09) \exp(-0.14(\pm 0.03) t), \quad \text{Eq. 13}$$

where *t* is time expressed in minutes and SE is presented in parentheses. The 2 methods of sampling displayed strong correlation (*R*² = 99%).

PET Experiments

Elevated CHC uptake in various organs in the abdominal cavity precluded use of this tracer for tumor analysis in this area. We therefore chose to grow tumors in the neck and

TABLE 2
Tissue Distribution of Radiolabel from ³H-, ¹⁴C-, and ¹¹C-CHC at 1 Hour After Injection

Tumor type	Tissues	³ H-CHC		¹⁴ C-CHC (n = 12)	¹¹ C-CHC (n = 6)	¹¹ C-CHC (Rats) (n = 4)
		High dose (n = 10)	Trace dose (n = 10)			
BE(2)-C	Liver	5.93 ± 0.59	10.07 ± 2.12	6.45 ± 0.74	2.09 ± 0.38	1.17 ± 0.60
	Spleen	4.67 ± 0.75	4.03 ± 1.31	3.94 ± 1.14	1.52 ± 0.41	0.69 ± 0.24
	Kidneys	7.31 ± 1.77	10.56 ± 3.78	1.89 ± 0.36	1.58 ± 0.37	0.62 ± 0.08
	Blood	1.15 ± 0.12	1.96 ± 0.43	1.48 ± 0.34	0.47 ± 0.16	0.02 ± 0.01
	Tumor	1.66 ± 0.15	1.84 ± 0.31	1.33 ± 0.19	1.50 ± 0.16	0.31 ± 0.08
BE(2)-C/CHC	Liver	6.27 ± 1.54	4.55 ± 0.68	6.41 ± 1.92	2.33 ± 0.43	1.41 ± 0.46
	Spleen	3.71 ± 0.28	3.59 ± 0.60	3.63 ± 1.15	1.97 ± 0.41	1.18 ± 0.22
	Kidneys	2.94 ± 0.54	3.45 ± 0.99	2.21 ± 0.65	1.62 ± 0.35	0.74 ± 0.14
	Blood	0.97 ± 0.16	1.20 ± 0.27	0.62 ± 0.16	0.46 ± 0.07	0.04 ± 0.01
	Tumor†	0.70 ± 0.09	0.79 ± 0.09	0.55 ± 0.11	0.48 ± 0.09	0.17 ± 0.02

*Determined in previous studies (26–28).

†*P* < 0.01 relative to BE(2)-C tumor by *t* test (planned comparison) for ³H-CHC; *P* < 0.05 relative to BE(2)-C tumor by *t* test (planned comparison) for ¹⁴C-CHC; *P* < 0.05 relative to BE(2)-C tumor by *t* test (planned comparison) for ¹¹C-CHC.

shoulder regions, where the background radiation of ^{11}C -CHC in surrounding tissue was expected to be low.

A representative ^{11}C -CHC image of a coronal section of a rat bearing resistant and sensitive tumors is shown in Figure 5. The image resembles those obtained previously with quantitative autoradiography and conforms to the biodistribution data. We found that CHC was rapidly excreted into the liver, spleen, and kidney and, in later stages of the experiment, into the urine and feces. The uptake was considerably lower everywhere away from the abdominal cavity, including in the extremities and head. The tumors were clearly visible in all images.

After each experiment the ^{11}C -CHC-associated tumor uptake was studied in a series of transaxial sections corresponding to consecutive time frames. To facilitate tumor localization we used FDG images. The FDG static images were taken approximately 100 min after ^{11}C -CHC injection (4.9 half-lives of ^{11}C), and only negligible ^{11}C activity was assumed to be present in tumor tissue at this time. The method of identifying and copying ROIs in analysis of PET images is shown in Figure 6. Because the anesthetized animals remained in a fixed position throughout the study, the geometric location of ROIs remained constant. This was verified by copying ROIs to static transmission scans performed at the start of the study.

The ^{11}C -CHC-associated activity was expressed as %ID/mL and plotted versus time. The results of experiments for 4 sensitive and 4 resistant tumors are presented in Figure 7. The maximum uptake at 1.5–2 min was followed by a rapid decrease throughout the study. The absolute uptake in resistant tumors was consistently about 2 times lower than that in sensitive tumors.

The overlaid dashed curve in Figure 7 represents the blood clearance of ^{11}C -CHC measured in a separate experiment. It is evident that, when compared with the tumor clearance curves, the blood clearance curve subdivides the time course of the study into 2 time segments of approximately 20 min each. During the first period the blood

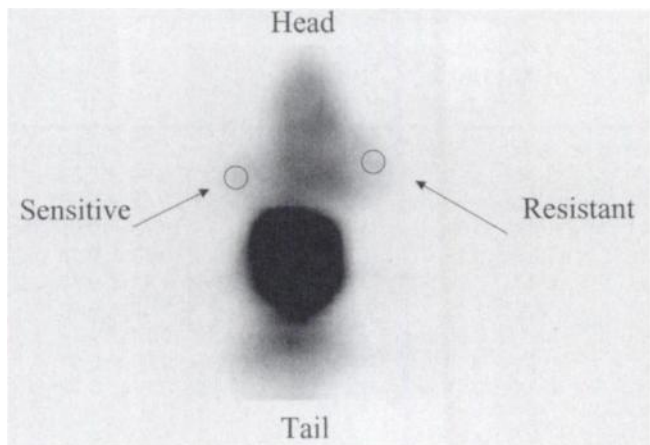


FIGURE 5. Representative coronal slice of rat bearing sensitive and resistant tumors. Section corresponds to 10 min after injection.

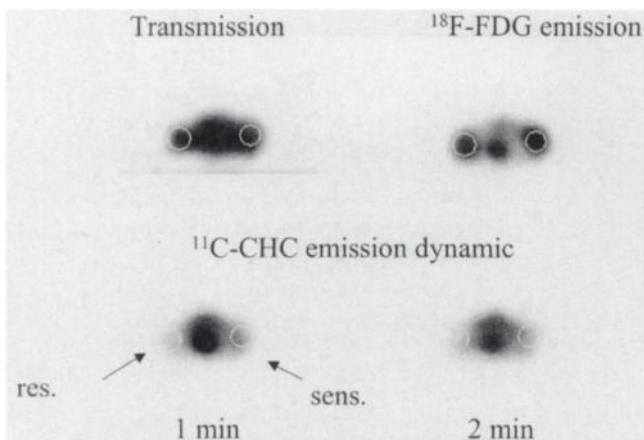


FIGURE 6. Method for ROI identification using FDG and transmission scans. ROIs are easily outlined on FDG and copied onto transmission and all ^{11}C -CHC emission scans. Animals were not moved throughout study, and geometric location of ROIs in all images was unchanged.

^{11}C -CHC content is significantly higher than the tumor content, and the tumor clearance kinetics are determined by the rate of blood clearance according to Equation 10. In the second period the blood ^{11}C -CHC content is significantly lower than that in tumors, and the tumor clearance kinetics are determined by dissociation of ^{11}C -CHC from intracellular targets according to Equation 12.

Equation 10 was used to fit the points obtained in the first 20 min, and Equation 12, to fit the points in the last 20 min. We found that in the first 20 min the data were best fitted ($R^2 = 99\%$) with the following variation of Equation 10:

$$\text{CHC} = [A/(k_{b1} - k_2)](\exp(-k_{21}t) - \exp(-k_{b1}t)) + B\exp(-k_{b2}t), \quad \text{Eq. 14}$$

where k_{b1} , k_{b2} , k_{21} , A , and B are parameters determined from

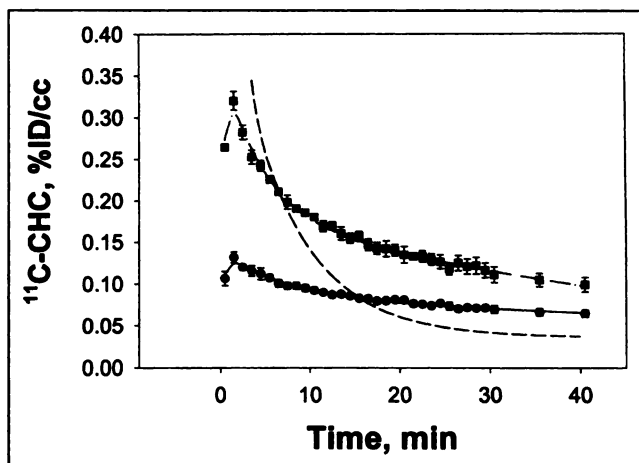


FIGURE 7. Data from dynamic ^{11}C -CHC scan plotted as function of time. Data are presented as average of tumors \pm SE. Data were fitted using theoretical equations as described in text. Dashed line represents blood clearance data presented in Figure 4. \blacksquare = sensitive BE(2)-C tumor; \bullet = resistant CHC(0.2) tumor.

the fitting procedure. Data from the last 20 min were best approximated ($R^2 = 95\%$) by the variation of Equation 12:

$$[\text{CHC}] = C \exp(-k_{22}t) + C_2, \quad \text{Eq. 15}$$

where C , C_2 , and k_{22} are parameters determined from fitting. The results of fitting are presented in Table 3. It is evident from comparison of the parameters that k_{b1} , k_{b2} , and C_2 are statistically the same in sensitive and resistant tumors. Moreover, k_{b1} is statistically the same as the higher rate of blood clearance reported above. We can thus interpret k_{b1} as the parameter determining CHC clearance from the blood pool in the tumor. The exponential term involving k_{b2} and B can be thought of as a composite of CHC blood clearance from the tumor blood pool and a transition term between the 2 regions of fitting. C_2 can be interpreted as a residual uptake in the tumors and the background from the surrounding tissue.

Parameter k_{21} and k_{22} are equal for sensitive tumors and statistically close for resistant tumors. Furthermore, k_{22} is equal to the rate of CHC accumulation observed in vitro in the cell lines used for xenografting, when these were exposed to various CHC concentrations (J. Lee, unpublished data, November 1999). These rates were found to be independent of concentration. We thus can interpret both these parameters as equal to parameter k_2 as used in the mathematic analysis. Indeed, this result follows from the mathematic model, because in the last 20 min of the experiment the blood clearance of CHC occurred much faster than CHC dissociation from tubulin, and Equation 10 is well approximated by a monoexponential decrease.

Finally, parameters A and C determine the absolute CHC uptake in the tumors. These parameters differ significantly (approximately 2-fold difference) in sensitive and resistant tumors.

These findings taken together confirm the general validity of the assumptions made in the mathematic model developed here. This allows us to assume parameter A to be proportional to the product of k_1T . Therefore, tumor resistance can be expressed as a proportional ratio ($r = k_2/A$). This ratio is proportional to the ratio of tubulin concentration and dissociation constant of tubulin-CHC interaction shown to be a measure of resistance in vitro (29). Indeed, the ratio of parameter r of resistant and sensitive cells is close to between 5 and 7, or equivalent to the value of approximately 7 determined in vitro.

TABLE 3

Parameters from Fitting PET Data to Modeling Equations

Parameter	Sensitive	Resistant
A, %ID/mL/min	0.39 ± 0.08	0.21 ± 0.04
B, %ID/mL	0.17 ± 0.05	0.05 ± 0.01
k_{b1} /min	1.73 ± 0.87	2.03 ± 0.38
k_{b2} /min	0.34 ± 0.16	0.31 ± 0.11
k_{21} /min	0.03 ± 0.01	0.02 ± 0.01
C, %ID/mL	0.15 ± 0.01	0.08 ± 0.04
k_{22} /min	0.03 ± 0.01	0.07 ± 0.03
C_2 , %ID/mL	0.06 ± 0.04	0.06 ± 0.01

DISCUSSION

^{11}C -CHC is described in this article as a potential diagnostic MDR tracer. Although other MDR tracers are currently being tested, it is likely that each will be well suited for modeling resistance to a specific group of compounds. Sestamibi distribution, for example, seems to model well uptake of various positively charged drugs. Transport of this compound may prove difficult to model, because various processes, such as prevalent accumulation in cell compartments with lower pH, efflux mediated by variations in membrane potential, and decreased target affinity, all can play a role in resistance. ^{11}C -CHC does not carry a charge, so its distribution is easier to analyze. In addition, as is evident from the cell resistance study reported here, resistance to CHC and another neutral drug, paclitaxel, is strongly correlated. This finding suggests that ^{11}C -CHC may be a good predictor of paclitaxel resistance.

The limitations of PET camera spatial resolution necessitated use of animals larger than the mice used in our previous studies. We therefore extended our biodistribution experiments to include nude rats xenografted with the same tumor lines. We found the results to be in good agreement with those obtained in our previously described experiments with mice (31). We again observed a significant difference between the label uptake in resistant versus sensitive tumors. The general feature of CHC biodistribution at 1 h after injection is elevated uptake in the liver, kidneys, and spleen. These results are consistent with the general view of CHC excretion through the bile and urine (33).

PET experiments resulted in a kinetic description of CHC uptake in tumors and other organs of interest. These data were subsequently compared with theoretically predicted functional dependencies, both to test applicability of the model developed in in vitro studies and to determine parameters convenient for resistance estimation in vivo. According to mathematical analysis the ratio of the tubulin concentration to the CHC-tubulin dissociation constant can serve as such a parameter. Parameter r , proportional to this ratio, can be determined by fitting experimental data to theoretical curves. The ratio of values of r found for tumors was the same as that found in vitro. This result justifies using r as the parameter characterizing resistance of a tumor as determined by PET.

In the fitting procedure we considered separately the initial rapid surge and decrease of CHC and the following slower clearance. This allowed us to obtain separate parameters, A (from the first fit) and k_2 (from the second fit). The rapid CHC blood clearance essentially means that the second fit describes dissociation of CHC from tubulin, with time constants close to those obtained in vitro. Therefore, a simple exponential fit produces k_2 values.

Although we could obtain very good agreement between the results observed in the PET studies and expected on the basis of in vitro experiments, the success of this technique might be explained in part by relatively high value of resistance in the CHC (0.2) line. Tumors in the clinic are likely to have lower values of resistance and might not be as

easily discernable. To further explore applicability and sensitivity of this method we plan to xenograft cell lines with considerably lower levels of resistance. We also plan to compare the bolus injection protocol used in this study with infusion. In infusion experiments we will attempt to maintain constant CHC plasma concentration long enough for the difference in the uptake between sensitive and resistant tumors to approach the limit seen in in vitro experiments (approximately 7 for the cell lines used in this study).

CONCLUSION

Our findings indicate that the method described here will be useful only for analysis of tumors away from the abdominal cavity. Though limiting, this requirement still leaves available for study a wide range of tumor locations, including the head, extremities, breast, lungs, and others.

Another limitation of ^{11}C -CHC prognostic imaging results from the electroneutrality of this agent. Electroneutrality is defined here as the property of remaining uncharged over a relatively wide range of pH values. (A variation of 1 unit around the level of 7.2 can be considered physiologically relevant.) Electroneutrality eliminates the role of the membrane potential as a factor in MDR, which makes the modeling of resistance considerably simpler. Other electro-neutral P-gp substrates include taxol and some steroid hormones. We have observed in vitro that, in the cell lines used in this study, levels of resistance to CHC and taxol are strongly correlated. We plan to investigate this relationship in PET experiments. We are also planning to investigate the relationship between distribution ^{11}C -CHC and another MDR imaging agent, sestamibi.

In addition to the analysis of its resistance to chemotherapeutic agents, ^{11}C -CHC imaging may provide important information about the efficacy of using CHC in the treatment of various abnormalities. CHC is currently used in therapy for acute gout and familial Mediterranean fever. It appears to be helpful in the treatment of Behçet's disease, liver cirrhosis, scleroderma, and others (37,38). Use of CHC imaging may help elucidate the pharmacologic action of this drug in the treatment of these abnormalities.

ACKNOWLEDGMENT

This work was supported by U.S. Department of Energy grant DE-FG02-86ER60407.

REFERENCES

- Beck WT. Mechanisms of multidrug resistance in human tumor cells: the roles of P-glycoprotein, DNA topoisomerase II, and other factors. *Cancer Treat Rev*. 1990;17(suppl):11-20.
- Bellamy T. P-glycoproteins and multidrug resistance. *Ann Rev Pharmacol Toxicol*. 1996;36:161-183.
- Gottesman MM, Pastan I, Ambudkar SV. P-glycoprotein and multidrug resistance. *Curr Opin Genet Dev*. 1996;6:610-617.
- Nooter K, Stoter G. Molecular mechanisms of multidrug resistance in cancer chemotherapy. *Pathol Res Pract*. 1996;192:768-780.
- Suto R, Abe Y, Nakamura M, et al. Multidrug resistance mediated by overexpression of P-glycoprotein in human osteosarcoma in vivo. *Int J Oncol*. 1998;12:287-291.
- Crankshaw CL, Marmion M, Luker GD, et al. Novel technetium (III)-Q complexes for functional imaging of multidrug resistance (MDR1) P glycoprotein. *J Nucl Med*. 1998;39:77-86.
- Piwnica-Worms D, Rao V, Kronauge J, Croop J. Characterization of multidrug resistance P-glycoprotein transport function with an organotechnetium cation. *Biochemistry*. 1993;34:12210-12220.
- Del Vecchio S, Ciarmiello A, Potena MI, et al. In vivo detection of multidrug-resistant (MDR1) phenotype by $^{99\text{m}}\text{Tc}$ -sestamibi scan in untreated breast cancer patients. *Eur J Nucl Med*. 1997;24:150-159.
- Del Vecchio S, Ciarmiello A, Pace L, et al. Fractional retention of $^{99\text{m}}\text{Tc}$ -sestamibi as an index of P-glycoprotein expression in untreated breast cancer patients. *J Nucl Med*. 1997;38:1348-1345.
- Ciarmiello A, Del Vecchio S, Silvestro P, et al. Tumor clearance of technetium-99m-sestamibi as a predictor of response to neoadjuvant chemotherapy for locally advanced breast cancer. *J Clin Oncol*. 1998;16:1677-1683.
- Hofmockel G, Bassukas ID, Wittmann A, Dammrich J. Is the expression of multidrug resistance gene product a prognostic indicator for the clinical outcome of patients with renal cancer? *Br J Urol*. 1997;80:11-17.
- Mansi L, Rambaldi PF, Cuccurullo V, et al. Diagnostic and prognostic role of $^{99\text{m}}\text{Tc}$ -tetrofosmin in breast cancer. *Q J Nucl Med*. 1997;41:239-250.
- Yuen AR, Sikic BI. Multidrug resistance in lymphomas. *J Clin Oncol*. 1994;12:2453-2459.
- Zhou DC, Zittoun R, Marie JP. Expression of multidrug resistance-associated protein (MRP) and multidrug resistance (MDR1) genes in acute myeloid leukemia. *Leukemia*. 1995;9:1661-1666.
- Haber M, Bordow SB, Haber PS, Marshall GM, Stewart BW, Norris MD. The prognostic value of MDR1 gene expression in primary untreated neuroblastoma. *Eur J Cancer*. 1997;33:2031-2036.
- Pogliani EM, Belotti D, Rivolta GF, Maffe PF, Corneo G. Anthracycline drugs and MDR expression in human leukemia. *Cytotechnology*. 1996;19:229-235.
- de Silva M, Kantharidis P, Wall DM, et al. Inheritance of chromosome 7 associated with a drug-resistant phenotype in somatic cell hybrids. *Br J Cancer*. 1996;73:169-174.
- Higgins CF, Callaghan R, Linton KJ, Rosenberg MF, Ford RC. Structure of the multidrug resistance P-glycoprotein. *Semin Cancer Biol*. 1997;8:135-142.
- Rosenberg MF, Callaghan R, Ford RC, Higgins CF. Structure of the multidrug resistance P-glycoprotein to 2.5 nm resolution determined by electron microscopy and image analysis. *J Biol Chem*. 1997;272:10685-10694.
- Beck WT, Grogan TM, Willman CL, et al. Methods to detect P-glycoprotein-associated multidrug resistance in patients' tumors: consensus recommendations. *Cancer Res*. 1996;56:3010-3020.
- Noonan KE, Beck C, Holzmayer TA, et al. Quantitative analysis of MDR1 (multidrug resistance) gene expression in human tumors by polymerase chain reaction. *Proc Natl Acad Sci USA*. 1990;87:7160-7164.
- Herzog CE, Trepel JB, Mickley LA, Bates SE, Fojo AT. Various methods of analysis of mdr-1/P-glycoprotein in human colon cancer cell lines. *J Natl Cancer Inst*. 1992;84:711-716.
- Kostakoglu L, Elahi N, Kiratli P, et al. Clinical validation of the influence of P-glycoprotein on technetium-99m-sestamibi uptake in malignant tumors. *J Nucl Med*. 1997;38:1003-1008.
- Piwnica-Worms D, Chiu ML, Budding M, Kronauge JF, Kramer RA, Croop JM. Functional imaging of multidrug-resistant P-glycoprotein with an organotechnetium complex. *Cancer Res*. 1993;53:977-984.
- Maffioli L, Steens J, Pauwels E, Bombardieri E. Applications of $^{99\text{m}}\text{Tc}$ -sestamibi in oncology. *Tumori*. 1996;82:12-21.
- Kostakoglu L, Kiratli P, Ruacan S, et al. Association of tumor washout rates and accumulation of technetium-99m-MIBI with expression of P-glycoprotein in lung cancer. *J Nucl Med*. 1998;39:228-234.
- Hendrikse NH, De Vries EGE, Schinke AH, et al. P-glycoprotein mediated pharmacokinetics of radiopharmaceuticals analyzed by positron emission tomography in vivo [abstract]. *Proc Am Assoc Cancer Res*. 1997;39:385.
- Hendrikse NH, De Vries EGE, Fluks E, van der Graaf WTA, Vaalburg W, Fransen EGF. P-glycoprotein mediated kinetics in tumor bearing rats with [^{11}C]daunorubicin and positron emission tomography [abstract]. *Proc Am Assoc Cancer Res*. 1998;39:71.

29. Roepe PD, Wei LY, Hoffman MM, Fritz F. Altered drug translocation mediated by the MDR protein: direct, indirect, or both? *J Bioenerg Biomembr*. 1996;28:541-555.
30. Wadkins RM, Roepe PD. Biophysical aspects of P-glycoprotein-mediated multidrug resistance. *Int Rev Cytol*. 1997;171:121-165.
31. Mehta BM, Levchenko A, Rosa E, et al. Evaluation of carbon-14-colchicine biodistribution with whole-body quantitative autoradiography in colchicine-sensitive and -resistant xenografts. *J Nucl Med*. 1996;37:312-314.
32. Mehta BM, Rosa E, Biedler JL, Larson SM. In vivo uptake of carbon-14-colchicine for identification of tumor multidrug resistance. *J Nucl Med*. 1994;35:1179-1184.
33. Mehta BM, Rosa E, Fissekis JD, Bading JR, Biedler JL, Larson SM. In-vivo identification of tumor multidrug resistance with ³H-colchicine. *J Nucl Med*. 1992;33:1373-1377, 1619.
34. Ferrand VL, Montero JF, Chauvet MM, Hirn MH, Bourdeaux MJ. Quantitative determination of the MDR-related P-glycoprotein, Pgp 170, by a rapid flow cytometric technique. *Cytometry*. 1996;23:120-125.
35. Fonti R, Levchenko A, Mehta BM, Zhang J, Tsuruo T, Larson SM. Measurement of P-glycoprotein expression in human neuroblastoma xenografts using in vitro quantitative autoradiography. *Nucl Med Biol*. 1999;26:35-41.
36. Kothari PJ, Finn RD, Larson SM. Syntheses of colchicine and isocolchicine labelled with carbon-11 and carbon-13. *J Label Comp Radiopharm*. 1995;36:521-528.
37. Levy M, Spino M, Read SE. Colchicine: a state-of-the-art review. *Pharmacotherapy*. 1991;11:196-211.
38. Famaey JP. Colchicine in therapy: state of the art and new perspectives for an old drug. *Clin Exp Rheumatol*. 1988;6:305-317.